

Novel Type of Superlattices Based on Gapless Graphene with the Alternating Fermi Velocity

P. V. Ratnikov and A. P. Silin

Lebedev Physical Institute, Russian Academy of Sciences, Moscow, 119991 Russia

e-mail: ratnikov@lpi.ru

Received July 1, 2014

We study a novel type of graphene-based superlattices formed owing to a periodic modulation of the Fermi surface. Such a modulation is possible for graphene deposited on a striped substrate made of materials with substantially different values of the dc permittivity. Similar superlattices appear also in graphene sheets applied over substrates with a periodic array of parallel grooves. We suggest a model describing such superlattices. Using the transfer-matrix technique, we determine the dispersion relation and calculate the energy spectrum of these superlattices. We also analyze at a qualitative level the current–voltage characteristics of the system under study.

DOI: 10.1134/S0021364014170123

1. INTRODUCTION

Graphene-based superlattices still attract considerable current interest. In particular, researchers deal with rippled graphene, which can be considered as a superlattice with a one-dimensional periodic potential related to these ripples [1]. The theoretical analysis was performed for superlattices arising under the effect of the applied periodic electrostatic potential [2] as well as of periodic arrays formed by magnetic barriers [3].

Graphene-based superlattices with a periodically modulated band gap were studied in [4]. This modulation is possible due to the interaction of graphene with the substrate material. Hexagonal boron nitride was chosen as such a material.

A similarity between the one-dimensional graphene-based superlattice and graphene exposed to a standing laser-produced light wave was demonstrated in [5]. The *ab initio* calculations of the electronic properties of superlattices formed by alternating of gapless graphene and graphene were reported in [6].

The Bloch-Zener oscillations in the superlattices formed by graphene and gapless HgTe semiconductor were studied in [7]. The splitting of the Landau levels in the graphene-based superlattice in a magnetic field applied perpendicularly to its surface was analyzed in [8]. Different types of semiconductor superstructures were described in detail in review [9].

The model of superlattice suggested in [4] was used in [10] to find the condition corresponding to the formation of additional Dirac points and Tamm minibands arising due to the intersection of the dispersion curves

of the gapless graphene and its gapped modification. This condition is in agreement with that obtained earlier for semiconductor heterostructures [11, 12]. The surface states in graphene-based heterostructures were analyzed in [13, 14].

In this paper, we suggest a novel type of superlattices based on gapless graphene with alternating regions characterized by different values of the Fermi velocity. In our case, the *Fermi velocity engineering* is based on the usage of the surrounding graphene materials, which have different values of permittivity [15]. The idea to control the Coulomb interaction between charge carriers in graphene by the choice of substrate materials with the necessary values of dc permittivity was first put forward in [16].

In such heterostructures, it is possible to achieve the energy quantization for charge carriers even in the absence of potential barriers (regions with wider band gaps) and quantum wells (regions with narrower band gaps), and even without any variations in the work function [17]. Note that low-energy (Tamm) minibands are absent here since the straight dispersion lines do not intersect anywhere except for the Dirac point.

Such structure can be produced by the deposition of graphene on striped substrates where either the composition (parameter x in an alloy) of SiO_{2-x} , or the density of some (nonmagnetic) impurities, or dc permittivity ϵ exhibit periodic variations. Here, we treat in detail the latter possibility.

According to the results of the theoretical [18–22] and experimental [15, 23–27] studies, the Fermi velocity becomes substantially renormalized. To estimate

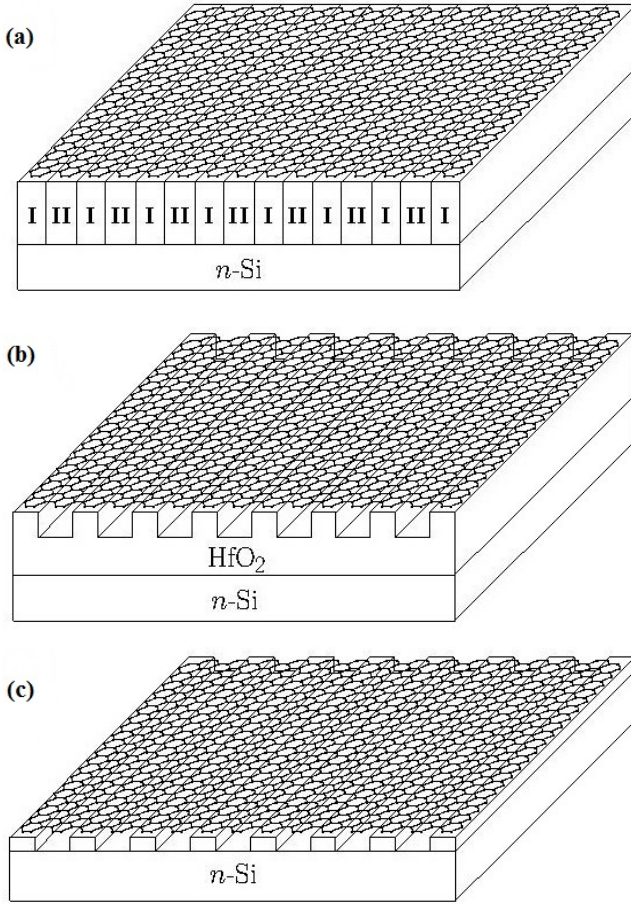


Fig. 1. Three variants of the superlattice under study: (a) graphene sheet placed on a striped substrate consisting of alternating layers of materials with substantially different values of the permittivity, e.g., SiO_2 with $\varepsilon = 3.9$ (I) and HfO_2 with $\varepsilon = 25$ (II); (b) graphene sheet placed on the HfO_2 substrate with periodically arranged grooves; and (c) graphene sheet deposited on a periodic array of parallel metallic strips. A plate of heavily doped silicon $n\text{-Si}$ is used as a gate.

the renormalized Fermi velocity, we can use the relation [20]

$$\frac{v_F}{v_{F0}} = 1 - 3.28\alpha^* \left[1 + \frac{1}{4} \ln \left(1 + \frac{1}{4\alpha^*} - 1.45 \right) \right],$$

where $\alpha^* = \tilde{e}^2/\hbar v_{F0}$ is the analog of the fine structure constant, v_{F0} is the initial unrenormalized Fermi velocity ($v_{F0} = 0.85 \times 10^8$ cm/s) [15, 26], $\tilde{e}^2 = e^2/\varepsilon_{eff}$, and $\varepsilon_{eff} = (\varepsilon_1 + \varepsilon_2)/2$ is the effective dc permittivity for the charge carriers in graphene depending on the values ε_1 and ε_2 of dc permittivity characterizing the materials surrounding graphene. Note that here the band gap is not open; this is confirmed in experiment with an accuracy of 0.1 meV [26].

Within the graphene region located over the strip with the lower value of ε , we have larger α^* . Hence, the corresponding renormalized Fermi velocity should be higher than that over the strip with the higher value of ε . This suggests the possibility of modulating v_F by varying the substrate permittivity. Note that such a system is a one-dimensional photonic crystal.

The first version of the suggested system is a graphene sheet placed on a striped substrate consisting of alternating layers of materials with substantially different values of the permittivity. A schematic image of such a system is shown in Fig. 1a.

It is also possible to use a substrate with periodically arranged grooves prepared by etching. The graphene sheet placed on such substrate should have the periodically alternating regions suspended over the grooves and those being in contact with the substrate material (see Fig. 1b). The renormalization of the Fermi velocity should be the most clearly pronounced just in the suspended graphene regions since here we have $\varepsilon_{eff} = 1$. According to the experimental data, the renormalized Fermi velocity in suspended graphene increases to 3×10^8 cm/s [26].

In the regions with graphene in contact with the narrow gap semiconducting material, where $\varepsilon_{eff} \gg 1$, the renormalized Fermi velocity differs only slightly from the unrenormalized one. In addition, the substrate itself is a diffraction grating. Therefore, the system should exhibit rather interesting optical characteristics, demanding a separate study.

There is another version of the system under study. It is possible to deposit graphene on a periodic array of parallel metallic strips (Fig. 1c). This is the limiting case: in the suspended graphene regions, we have $\varepsilon_{eff} = 1$ (the strongest renormalization of the Fermi velocity), whereas in the regions with graphene in contact with metallic strips, we have $\varepsilon_{eff} = \infty$ (vanishing renormalization of the Fermi velocity [15]).

We see that a whole class of such type of systems, which were not studied earlier, is possible. Without doubt, the studies of such systems should lead to important advances in the implementation of the technologies based on the controlled Fermi velocity.

2. MODEL

The model for the description of the suggested superlattice is similar to that used earlier to study the superlattice on the striped substrate with the periodic variation in the band gap [4].

In our case, we assume that the band gap remains unchanged and is equal to zero (gapless graphene) and the work function is the same over all regions of the superlattice (its value is chosen as the energy reference point). We have only a modulation of the Fermi velocity. In gapless graphene, a change in the work function leads to the electrical breakdown and to the creation of electron-hole pairs. We also assume that the near-border region corresponding to the gradual change in the Fermi velocity is much narrower than the superlattice period. Therefore, the v_F profile can be considered to be sharp enough (see Fig. 2).

We consider the charge carriers located close to the K point of the Brillouin zone (the results should be the same for the charge carriers located in the vicinity of the K' point). Let the x axis be perpendicular to

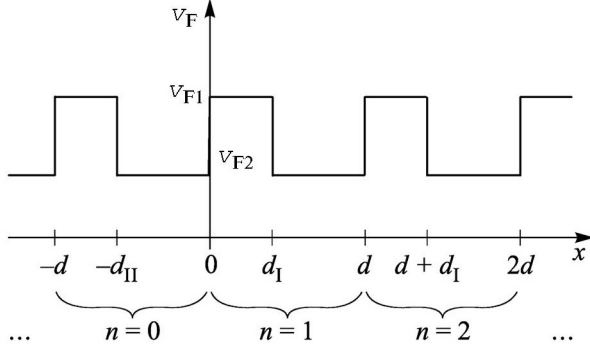


Fig. 2. Fermi velocity profile in the superlattice under study ($v_{F1} > v_{F2}$ case). The enumeration of supercells in the superlattice and the sizes of its regions are indicated in the lower part of the figure: d_I is the width of the graphene strip with the Fermi velocity v_{F1} , d_{II} is the width of the graphene strip with the Fermi velocity v_{F2} , and $d = d_I + d_{II}$ is the period of the superlattice.

the strips as is shown in Fig. 2. The envelope of the wave-function $\Psi(x, y)$ for the charge carriers obeys the Dirac-Weyl equation with variable Fermi velocity¹

$$v_F \sigma \hat{p} \Psi(x, y) = E \Psi(x, y), \quad (1)$$

$$v_F = \begin{cases} v_{F1}, & d(n-1) < x < -d_{II} + dn \\ v_{F2}, & -d_{II} + dn < x < dn. \end{cases} \quad (2)$$

Here, $\hat{p} = -i\nabla$ is the momentum operator (here and further on, $\hbar = 1$). Integers n enumerate supercells (see Fig. 2). The Pauli matrices $\sigma = (\sigma_x, \sigma_y)$ act in the space of two sublattices. The motion of charge carriers in the superlattice along the y axis is free; hence, a solution to Eq. (1) has the form $\Psi(x, y) = \psi(x)e^{ik_y y}$.

Similarly to [4], we find a solution of Eq. (1) with respect to $\psi(x)$ for the n th supercell

(i) at $0 < x < d_I$

$$\psi_n^{(1)}(x) = \Omega_{k_1}(x) \begin{pmatrix} a_n^{(1)} \\ c_n^{(1)} \end{pmatrix},$$

$$\Omega_{k_1}(x) = N_{k_1} \begin{pmatrix} 1 & 1 \\ \lambda_+^{(1)} & -\lambda_-^{(1)} \end{pmatrix} e^{ik_1 x \sigma_z},$$

$$\lambda_{\pm}^{(1)} = \frac{v_{F1}(k_1 \pm ik_y)}{E}, \quad k_1 = \frac{\sqrt{E^2 - v_{F1}^2 k_y^2}}{v_{F1}},$$

¹In the general case, one should write the anticommutator of the Fermi velocity $v_F(x)$ with the term containing the momentum operator \hat{p}_x

$$\frac{1}{2} \{v_F(x), \sigma \hat{p}\} \Psi(x, y) = E \Psi(x, y).$$

Such symmetrization of the Hamiltonian is necessary for retaining its Hermitian form. Similar problems were considered in [28, 29]. In the case of the stepwise profile (2) of the Fermi velocity, we obtain the equation for $\Psi(x, y)$ in form (1). This limitation is not significant since allowance for a smooth dependence $v_F(x)$ will complicate the calculations, but will insignificantly change the final results.

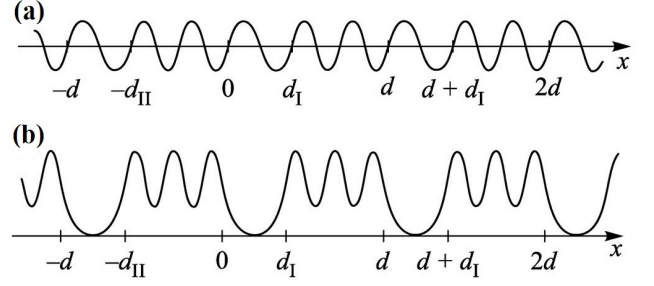


Fig. 3. Schematic image illustrating the behavior of the envelope of the wavefunction of charge carriers in the superlattice under study: (a) the oscillatory solution in all regions and (b) the solution being oscillatory in one region and exhibiting exponential decay deep into another region ($v_{F1} > v_{F2}$ case).

(ii) at $d_I < x < d$

$$\psi_n^{(2)}(x) = \Omega_{k_2}(x) \begin{pmatrix} a_n^{(2)} \\ c_n^{(2)} \end{pmatrix},$$

$$\Omega_{k_2}(x) = N_{k_2} \begin{pmatrix} 1 & 1 \\ \lambda_+^{(2)} & -\lambda_-^{(2)} \end{pmatrix} e^{ik_2 x \sigma_z},$$

$$\lambda_{\pm}^{(2)} = \frac{v_{F2}(k_2 \pm ik_y)}{E}, \quad k_2 = \frac{\sqrt{E^2 - v_{F2}^2 k_y^2}}{v_{F2}}.$$

Here, N_{k_1} and N_{k_2} are the normalization factors.

For the case $v_{F1} > v_{F2}$, the condition for the existence of the solution of Eq. (1), which oscillates in all regions of the superlattice (it is schematically illustrated in Fig. 3a), is reduced to the inequality

$$k_2^2 > \left(\frac{v_{F1}^2}{v_{F2}^2} - 1 \right) k_y^2. \quad (3)$$

The existence of a *solution of the mixed type* is also possible (see Fig. 3b). In this case, we have an oscillatory solution in some regions (effective quantum wells), whereas in the other regions, it exhibits exponential decay (effective potential barriers) deep into these regions. The condition for the existence of the mixed type solution is determined by the inequality inverse to (3) and it is met only for finite k_y values.

The effective quantum barrier of the new type is the region with the higher Fermi velocity because the energy of the charge carriers with the same momentum \mathbf{k} in it is higher than that in the effective quantum well with the lower Fermi velocity [17]. In contrast to the usual quantum well, which is formed owing to the change in the width of the band gap, the height of the barrier in the superlattice under study grows with k_y . At $k_y = 0$, the barrier vanishes and our problem is reduced to the *empty lattice model* [30]. In the latter model, the potential is absent, but the periodicity is retained. As a result, energy bands corresponding to the symmetry of the problem arise, but we have zero band gaps.

3. DISPERSION RELATIONS

To derive the dispersion relations, we use the transfer matrix (T -matrix) method in the way similar to that employed in [4].

The transfer matrix determines the relation between the coefficients appearing in the expressions for the envelopes of the wavefunctions for the neighboring supercells

$$\begin{pmatrix} a_{n+1}^{(1)} \\ c_{n+1}^{(1)} \end{pmatrix} = T \begin{pmatrix} a_n^{(1)} \\ c_n^{(1)} \end{pmatrix}, \quad \begin{pmatrix} a_{n+1}^{(2)} \\ c_{n+1}^{(2)} \end{pmatrix} = T \begin{pmatrix} a_n^{(2)} \\ c_n^{(2)} \end{pmatrix}.$$

We use the following boundary conditions for matching of the envelopes of the wavefunctions [14, 31],

$$\sqrt{v_{F1}}\psi_n^{(1)} = \sqrt{v_{F2}}\psi_n^{(2)},$$

and also the Bloch conditions in the form

$$\psi_n^{(1)}(x+d) = \psi_n^{(1)}(x)e^{ik_x d}$$

and

$$\psi_n^{(2)}(x+d) = \psi_n^{(2)}(x)e^{ik_x d}.$$

Then, the expression for the T -matrix has the form [4]

$$T = \Omega_{k_1}^{-1}(0)\Omega_{k_2}(d)\Omega_{k_2}^{-1}(d_I)\Omega_{k_1}(d_I).$$

The dispersion relation is determined from the equality

$$\text{Tr}T = 2\cos(k_x d),$$

which for the oscillatory type solution, can be written as

$$\begin{aligned} & \frac{v_{F1}v_{F2}k_y^2 - E^2}{v_{F1}v_{F2}k_1k_2} \sin(k_1 d_I) \sin(k_2 d_{II}) \\ & + \cos(k_1 d_I) \cos(k_2 d_{II}) = \cos(k_x d). \end{aligned} \quad (4)$$

For the solution of the mixed type, the dispersion relation is found from (4) through the use of the formal substitution $k_1 \rightarrow i\kappa_1$, where $\kappa_1 = \frac{1}{v_{F1}}\sqrt{v_{F1}^2 k_y^2 - E^2}$.

At $k_y = 0$, transcendental equation (4) has the form

$$\cos(k_1 d_I + k_2 d_{II}) = \cos(k_x d) \quad (5)$$

for which the exact solution can be found

$$E_l(k_x) = \pm v_F^* \left(k_x + \frac{2\pi l}{d} \right), \quad l = 0, 1, 2, \dots$$

Here, the effective Fermi velocity is introduced as

$$v_F^* = \frac{v_{F1}v_{F2}d}{v_{F1}d_{II} + v_{F2}d_I}. \quad (6)$$

For the l th miniband, the energy at the K point is equal to

$$E_l^0 = \pm \frac{2\pi l v_F^*}{d}, \quad l = 0, 1, 2, \dots$$

We can see that the lower electron miniband ($l = 0$) touches the upper hole miniband at the K point and graphene remains gapless.

From Eq. (5), we find that, at the edge of the l th miniband, the energy at $k_x = \pm\pi/d$ is equal to

$$E_l\left(\pm\frac{\pi}{d}\right) = \pm \frac{\pi(2l+1)v_F^*}{d}, \quad l = 0, 1, 2, \dots$$

The minibands are separated by the direct band gaps

$$E_G = E_{l+1}\left(\pm\frac{\pi}{d}\right) - E_l\left(\pm\frac{\pi}{d}\right) = \frac{2\pi v_F^*}{d}.$$

In the case of $k_y = 0$, indirect gaps are absent

$$E_l\left(\frac{\pi}{d}\right) = E_{l+1}\left(-\frac{\pi}{d}\right),$$

which corresponds to the empty lattice model [30].

4. NUMERICAL CALCULATION OF THE ENERGY SPECTRUM

Let us calculate the lower electron miniband for the superlattice shown in Fig. 1c. According to [26], for it we have $v_{F1} = 3 \times 10^6$ cm/s (suspended graphene) and $v_{F2} = 0.85 \times 10^6$ cm/s (in the region with the contact of graphene with the metal, the Fermi velocity coincides with v_{F0}).

In the weak coupling model, the problem concerning the edge type at the interface turns out to be unimportant. Let us assume that we have a zigzag-type boundary at the interface (see Fig. 1) and, in each of two regions of the supercell, integer numbers N_I and N_{II} of graphene unit cells are packed up. Then, we have $d_I = 3N_I a$ and $d_{II} = 3N_{II} a$, where $a = 1.42$ Å is the lattice constant of graphene. For calculations, we assume that $N_I = N_{II} = 50$, i.e., $d_I = d_{II} = 21.3$ nm.

In the framework of the suggested model, it is necessary to introduce the upper limit on the wave vector component characterizing the free motion of charge carriers, $|k_y| \ll k_c$. Momentum k_c corresponds to the energy of the ultraviolet cutoff, $\Lambda \approx 3$ eV [26]. As a result, we find $k_c \approx 4.3$ nm⁻¹. This, in turn, imposes the limitation on the superlattice period, $d \gg a$.

The results of numerical calculations are represented in the form of two $E(k_x, k_y)$ plots for the lower electron miniband: (i) $E(k_x)$ at fixed values of k_y (Fig. 4a) and (ii) $E(k_y)$ at fixed values of k_x (Fig. 4b). In Fig. 4a, we can see, in particular, that $k_y = 0$ corresponds to the linear dispersion law and the effective Fermi velocity is $v_F^* \approx 1.325 \times 10^8$ cm/s. The lower curve in Fig. 4b exhibits a nearly linear growth. This means that the $E(k_x, k_y)$ surface has the conical shape near the Dirac point.

Thus, we confirm by numerical calculations that at $k_y = 0$, the Fermi velocity of electrons (holes) has a constant value, does not vanish up to the boundaries of minibands, and is determined by Eq. (6) (this is true for all minibands). In this sense, the particles do not feel the boundaries of minibands. Note that, for $k_y \neq 0$, the velocity of particles always vanishes at the miniband boundaries.

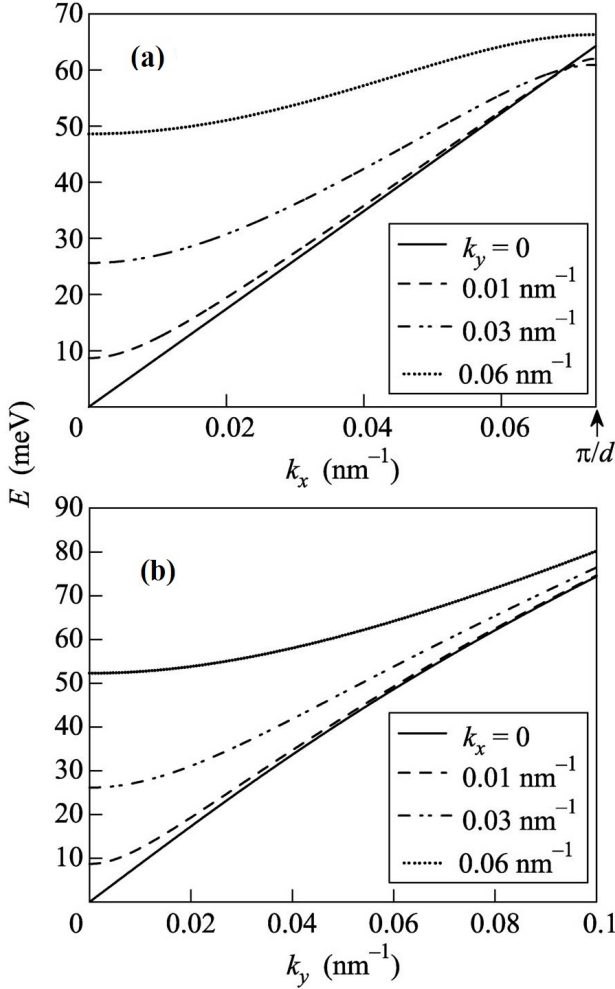


Fig. 4. Numerical calculation of the dispersion curves for the lower electron miniband (a) versus k_x at fixed k_y values and (b) versus k_y at fixed k_x values.

5. CURRENT-VOLTAGE CHARACTERISTICS (QUALITATIVE ANALYSIS)

Let us briefly discuss at the qualitative level the effect of the superlattice potential on the transport phenomena.

Having in mind the aforementioned qualitative difference between the $k_y = 0$ and $k_y \neq 0$ cases, we should expect that the current-voltage characteristics (I - V curves) of the superlattice under study should be significantly different for these two cases.

At $k_y = 0$, the transport characteristics of the superlattice under study should be the same as for effective gapless graphene with the average Fermi velocity v_F^* given by Eq. (6). In particular, at any arbitrarily low charge carrier density, we should observe nonzero minimum conductivity σ_{min} . According to the experimental data, we have $\sigma_{min} = 4e^2/h$ [32], which coincides with the ballistic conductivity of graphene. The I - V curve should exhibit a linear growth similar to that characteristic of graphene samples with high enough mobility of charge carriers, $\mu \gtrsim 10^4 \text{ cm}^2/(\text{Vs})$ [33].

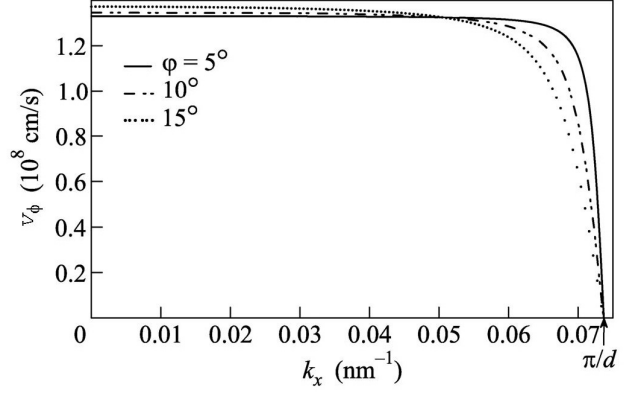


Fig. 5. Numerical calculation of the electron velocity in the lower miniband along the direction specified by the fixed polar angle ϕ .

In the case of $k_y \neq 0$, the situation is more complicated. At a nonzero transverse field V_y and at a sufficiently small longitudinal field V_x , the I - V curve should be a growing one and the differential conductivity at small values of V_x is about or higher than the minimum conductivity

$$\sigma_{dif}(V_x \approx 0) \gtrsim \sigma_{min}.$$

Now, we calculate the velocity of electrons for the case of fixed longitudinal (\mathcal{E}_x) and nonzero transverse (\mathcal{E}_y) electric fields. For the corresponding implementation of such situation in experiment, it is possible to use the standard Hall layout.

For simplicity, we assume that transport is ballistic; i.e., the mean free path λ is so large that an electron accelerated by the applied electric field can reach the miniband boundary without any scattering. To distinguish the spectrum related to the potential of the superlattice, the mean free path should be much larger than the period of the superlattice [34]

$$\lambda \gg d. \quad (7)$$

For the sufficiently pure graphene samples, we have $\lambda \simeq 1 \mu\text{m}$ [35].

The direction of the electron motion is characterized by the polar angle $\phi = \arctan(k_y/k_x)$. Its value remains unchanged in the whole $-\pi/d \leq k_x \leq \pi/d$ range. The contribution to the conductivity related to the intraminiband transitions is determined by the electron velocity, which we seek:

$$v_\phi = \left. \frac{\partial E}{\partial k} \right|_{k_y = k_x \tan \phi}.$$

In Fig. 5, we illustrate the calculated dependence of the electron velocity on k_x for the same superlattice parameters as above for the polar angles $\phi = 5^\circ, 10^\circ$, and 15° . We can see that the velocity indeed vanishes at the miniband boundary and its abrupt decrease takes place within a quite narrow range near the miniband boundary. For low momenta, we have $v_\phi \approx v_F^*$.

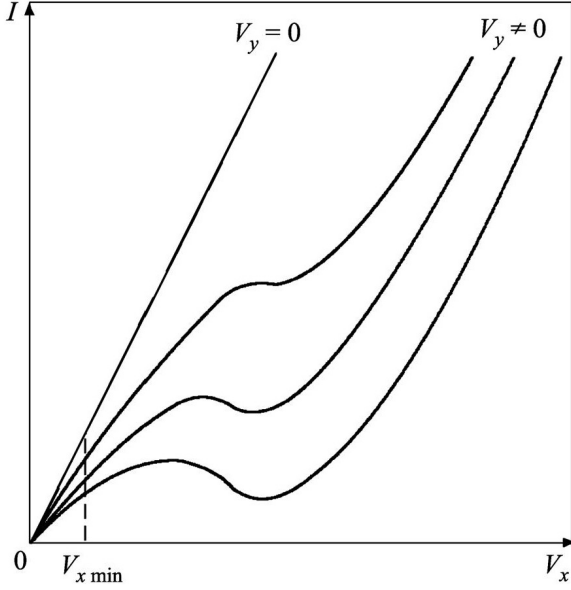


Fig. 6. Qualitative behavior of the I - V curve for the superlattice under study. Three $I(V_x)$ plots under the linear I - V curve correspond to the growth of the transverse voltage V_y (from top to bottom).

An application of the superlattice at nonzero temperatures requires the existence of a quite clearly pronounced Fermi velocity profile; i.e., we should use rather large ϕ and $\delta v_F = |v_{F1} - v_{F2}|$ values:

$$\pi \frac{\delta v_F}{d} \sin \phi \gg T.$$

However, at large ϕ values close to $\pi/2$, the condition according to which charge carriers pass a large number of supercells at the mean free path can be violated. Then, condition (7) turns out to be unimportant (condition $l \cos \phi \gg d$ should be met).

Similarly to the situation occurring in semiconductor superlattices, the motion of charge carriers at sufficiently strong electric field \mathcal{E}_x is finite. They oscillate with the Stark frequency [7, 34]

$$\Omega = e\mathcal{E}_x d.$$

This stems from the nonlinearity of the I - V curve manifesting itself in the negative differential conductivity at a certain section of it. Charge carriers in the nonlinear regime undergo a large number of the Bloch oscillations during the mean free time τ :

$$\Omega\tau \gg 1. \quad (8)$$

We estimate the mean free time as $\tau \approx \lambda/v_F^*$ (the velocity of charge carriers is $v_\phi \approx v_F^*$ everywhere except for a narrow range near the miniband boundaries). Then, condition (8) can be rewritten as

$$\mathcal{E}_x \gg \frac{v_F^*}{ed\lambda}. \quad (9)$$

Condition (9) automatically gives an estimate for the minimum longitudinal voltage above which negative

differential conductivity becomes possible

$$V_{x \min} \simeq \frac{v_F^* L_x}{ed \lambda},$$

where L_x is the size of the system along the x axis. Assuming that $L_x \simeq \lambda$, we arrive at the estimate $V_{x \min} \simeq 0.02$ V for the superlattice with the same parameters as above.

In Fig. 6, we represent the qualitative behavior of the I - V curve for the superlattice under study. At $k_y = 0$ (zero applied voltage in the transverse direction, $V_y = 0$), we observe its linear growth. At $k_y \neq 0$ (nonzero transverse voltage, $V_y \neq 0$), a section with negative differential conductivity arises in the curve. In this case, for higher V_y values, this section is more pronounced and more shifted toward lower V_x values. However, as is mentioned above, this section can arise only at a sufficiently high longitudinal voltage

$$V_x \gg V_{x \min}.$$

Note finally that the characteristics of the system under study can depend on the gate voltage V_g (at different values of the charge carrier density n_{2D}) owing to the dependence of the renormalized Fermi velocity on n_{2D} [26, 27]. In this case, a controlling factor is the filling of minibands with electrons (holes). For the experimental observations, it is convenient to have partially filled either the lower electronic miniband or the upper hole one (in this case, the higher electronic or lower hole minibands are distinguishable). This takes place if $n_{2D} \ll n_{2D}^* = 4/d^2$. This condition can be rewritten in the form of a limitation imposed on the gate voltage

$$|V_g| \ll 4\pi en_{2D}^* L_g / \varepsilon_s^*,$$

where L_g is the gate thickness and ε_s^* is the effective dc permittivity of the substrate. For the layered substrate structure (see Fig. 1a), we have

$$\varepsilon_s^* = \frac{\varepsilon_{s1} d_I + \varepsilon_{s2} d_{II}}{d}.$$

6. CONCLUSIONS

We suggested a novel class of graphene-based systems, which are at the same time both photon crystals and graphene superlattices with periodically varying Fermi velocity. Such a modulation appears to be possible owing to the renormalization of the Fermi velocity in the energy spectrum of graphene. New prospects become open for the implementation of the technologies based on controlled Fermi velocity. We point out some specific features of the transport phenomena in such systems, in particular, appearance of the sections with negative differential conductivity in the I - V curves. It is clear that, similarly to photon crystals, these systems should exhibit interesting optical characteristics.

References

- [1] A. Isacsson, L. M. Jonsson, J. M. Kinaret, and M. Jonson, Phys. Rev. B **77**, 035423 (2008).
- [2] C. Bai and X. Zhang, Phys. Rev. B **76**, 075430 (2007).
- [3] M. R. Masir, P. Vasilopoulos, A. Matulis, and F. M. Peeters, Phys. Rev. B **77**, 235443 (2008).
- [4] P. V. Ratnikov, JETP Lett. **90**, 469 (2009).
- [5] S. E. Savel'ev and A. S. Alexandrov, Phys. Rev. B **84**, 035428 (2011).
- [6] J.-H. Lee and J. C. Grossman, Phys. Rev. B **84**, 113413 (2011).
- [7] V. Krueckl and K. Richter, Phys. Rev. B **85**, 115433 (2012).
- [8] G. Pal, W. Apel, and L. Schweitzer, Phys. Rev. B **85**, 235457 (2012).
- [9] P. B. Sorokin and L. A. Chernozatonskii, Phys. Usp. **56**, 105 (2013).
- [10] G. M. Maksimova, E. S. Azarova, A. V. Telezhnikov, and V. A. Burdov, Phys. Rev. B **86**, 205422 (2012).
- [11] A. V. Kolesnikov, R. Lipperheide, A. P. Silin, and V. Wille, Europhys. Lett. **43**, 331 (1998).
- [12] E. A. Andryushin, A. P. Silin, and S. A. Vereshchagin, Phys. Low-Dim. Struct. **314**, 79 (2000).
- [13] P. V. Ratnikov and A. P. Silin, Phys. Solid State **52**, 1763 (2010).
- [14] P. V. Ratnikov and A. P. Silin, J. Exp. Theor. Phys. **114**, 512 (2012).
- [15] C. Hwang, D. A. Siegel, S.-K. Mo, W. Regan, A. Ismach, Y. Zhang, A. Zettl, and A. Lanzara, Sci. Rep. **2**, 590 (2012).
- [16] P. V. Ratnikov, JETP Lett. **87**, 292 (2008).
- [17] A. V. Kolesnikov and A. P. Silin, J. Exp. Theor. Phys. **82**, 1145 (1996).
- [18] J. Gonzalez, F. Guinea, and M. A. H. Vozmediano, Nucl. Phys. B **424**, 595 (1994).
- [19] J. Gonzalez, F. Guinea, and M. A. H. Vozmediano, Phys. Rev. B **59**, 2474 (1999).
- [20] S. Das Sarma, E. H. Hwang, and W.-K. Tse, Phys. Rev. B **75**, 121406(R) (2007).
- [21] M. S. Foster and I. L. Aleiner, Phys. Rev. B **77**, 195413 (2008).
- [22] F. de Juan, A. G. Grushin, and M. A. H. Vozmediano, Phys. Rev. B **82**, 125409 (2010).
- [23] A. Bostwick, T. Ohta, J. L. McChesney, T. Seyller, K. Horn, and E. Rotenberg, Solid State Commun. **143**, 63 (2007).
- [24] Z. Q. Li, E. A. Henriksen, Z. Jiang, Z. Hao, M. C. Martin, P. Kim, H. L. Stormer, and D. N. Basov, Nature Phys. **4**, 532 (2008).
- [25] G. Li, A. Luican, and E. Y. Andrei, Phys. Rev. Lett. **102**, 176804 (2009).
- [26] D. C. Elias, R. V. Gorbachev, A. S. Mayorov, S. V. Morozov, A. A. Zhukov, P. Blake, L. A. Ponomarenko, I. V. Grigorieva, K. S. Novoselov, F. Guinea, and A. K. Geim, Nature Phys. **7**, 701 (2011).
- [27] J. Chae, S. Jung, A. F. Young, C. R. Dean, L. Wang, Yu. Gao, K. Watanabe, T. Taniguchi, J. Hone, K. L. Shepard, Ph. Kim, N. B. Zhitenev, and J. A. Stroscio, Phys. Rev. Lett. **109**, 116802 (2012).
- [28] M. R. Geller and W. Kohn, Phys. Rev. Lett. **20**, 3103 (1993).
- [29] A. V. Kolesnikov and A. P. Silin, Phys. Rev. B **95**, 7596 (1999).
- [30] J. Callaway, Energy Band Theory (Academic, New York, 1964; Mir, Moscow, 1969).
- [31] A. P. Silin and S. V. Shubenkov, Phys. Solid State **40**, 1223 (1998).
- [32] K. S. Novoselov, A. K. Geim, S. V. Morozov, D. Jiang, M. I. Katsnelson, I. V. Grigorieva, S. V. Dubonos, and A. A. Firsov, Nature **438**, 197 (2005).
- [33] N. Vandecasteele, A. Barreiro, M. Lazzeri, A. Bachtold, and F. Mauri, Phys. Rev. B **82**, 045416 (2010).
- [34] A. P. Silin, Sov. Phys. Usp. **28**, 972 (1985).
- [35] K. I. Bolotin, K. J. Sikes, Z. Jiang, M. Klima, G. Fudenberg, J. Hone, P. Kim, H. L. Stormer, Solid State Commun. **146**, 351 (2008).

Translated by K. Kugel